Gaussian Belief Propagation for mmWave Large MIMO Detection with Low-Resolution ADCs

Itsuki Watanabe *, Takumi Takahashi *, Shinsuke Ibi †, Antti Tölli ‡, and Seiichi Sampei *
*Graduate School of Engineering, Osaka University, Yamada-oka 2–1, Suita, 565–0871, Japan
† Faculty of Science and Engineering, Doshisha University, 1–3 Tataramiyakodani, Kyotanabe, 610–0394, Japan
‡ Centre for Wireless Communications (CWC), FI-90014 University of Oulu, Finland
Email: *{watanabe@wcs., takahashi@, sampei@}comm.eng.osaka-u.ac.jp, †sibi@mail.doshisha.ac.jp, ‡antti.tolli@oulu.fi

***Abstract*—We propose a novel message passing de-quantization (MPDQ) algorithm for low-complexity uplink signal detection in mmWave large multi-user multi-input multi-output (MU-MIMO) systems with low-resolution analog-to-digital converters (ADCs) suffering from severe quantization errors. The proposed method consists of a de-quantization (DQ) step based on the Bussgang theorem and a Bayesian multi-user detection (MUD) via Gaussian belief propagation (GaBP), which detects the uplink signal while compensating for the quantized signal distortion. The efficacy is demonstrated by simulation results, which are shown to significantly outperform the current state-of-the-art (SotA) detection designed by Bussgang minimum mean square error (BMMSE) and generalized approximate message passing (GAMP) frameworks in 1-bit quantization, and approach the matched filter bound (MFB) performance.**

***Index Terms*—mmWave Large MIMO detection, belief propagation, low-resolution ADCs, Bussgang's theorem**

I. Introduction

Millimeter-wave (mmWave) large multi-user multi-input multi-output (MU-MIMO), which exploits a wide range of frequency bands to boost the data rates, has been intensively developed with the aim of commercializing fifth generation (5G) advanced and sixth generation (6G) networks.The short wavelength at mmWave frequency allows us to pack many antenna elements into a small area, and the resulting significant amount of spatial degrees of freedom (DoF) serves high spectral efficiency and massive connectivity.

However, fully digital and high-resolution large MIMO arrays will become increasingly distant to reality [1], owing to excessive power consumption and hardware cost. In uplink scenarios, every antenna element of a base station (BS) is equipped with a dedicated radio frequency (RF) chain that includes two analog-to-digital converters (ADCs), where the power consumption increases *exponentially* with the (effective) number of quantization bits [2]. For this reason, employing low-resolution ADCs with 1–2 bits of quantization instead of typical 6+ bits in each I/Q axis allows us to implement large MIMO arrays consisting of massive antenna elements required to operate in the mmWave frequency band [3]–[5].

In light of the above, this study focuses on a low-complexity and high-accuracy large multi-user detection (MUD) scheme based on the output of low-resolution ADCs with perfect channel state information (CSI) (please refer to, *e.g.*, [3], [4], [6]–[8] for actual channel estimation based on the quantized measurements). In mmWave MIMO channels, MUD suffers from high spatial fading correlations due to the small angular spread at the BS; however, it is computationally infeasible to use an optimal maximum likelihood (ML) detector [9] or its variants, *e.g.*, [10], in large MIMO setting. Spatial filtering based on Bussgang's theorem [11] is well known as a low-complexity estimation strategy [3]–[5], [12]. However, excessive reduction of the number of quantization bits, *i.e.*, the use of 1-bit quantization ADCs, induces a high-level error floor in bit error rate (BER) performance.

A promising approach to tackle this issue is Bayesian message passing de-quantization (MPDQ) on the basis of belief propagation (BP) [13]–[16], whose underlying unified inference framework is summarized in [17]. For high-dimensional MIMO channels, generalized approximate message passing (GAMP) approach [14], [15] consisting of only tensor products is preferable in terms of computational cost. However, the derivation heavily relies on the large-system approximation based on independent and identically distributed (i.i.d.) random measurements with zero mean, which makes it extremely vulnerable to the spatial fading correlation. To elaborate further, errors in *Onsager* term [14] for decoupling the self-feedback of message across iterations make the iterative convergence behavior unstable, resulting in performance degradation.

In order to resolve the lack of an appropriate MUD scheme for mmWave large MU-MIMO systems with low-resolution ADCs, this paper proposes a novel MPDQ algorithm via Gaussian belief propagation (GaBP) [18] employing Bussgang theorem. The GaBP approach can be interpreted as the origin of the aforementioned GAMP rules, and it possesses robustness to deviations from the ideal measurement condition by relaxing the dependence on the large-system limit approximation [19], in exchange for a slight increase in the number of tensor product operations. The efficacy of the proposed MPDQ algorithm is confirmed by numerical simulations, which shows that the proposed method not only outperforms the state-of-the-art (SotA), such as Bussgang minimum mean square error (BMMSE) and GAMP-based MPDQ, but also approaches a matched filter bound (MFB) in terms of BER.

Throughout this paper, vectors and matrices are denoted by lower- and upper-case bold-face letters, respectively. $\mathbb{R}^{a\times b}$ and $\mathbb{C}^{a\times b}$ denote real and complex fields of size $a\times b$. $\cdot^*$, $\cdot^{\mathrm{T}}$, and $\cdot^{\mathrm{H}}$ are the conjugate, transpose, and conjugate transpose operators, respectively. $p_{\mathsf{a}|\mathsf{b}}(a|b)$ represents the probability density function (PDF) of a realization a of random variable a given the occurrence of a realization b of random variable b. $\mathbb{E}_{\mathsf{a}}\{\cdot\}$ is the expected value of random variable a. $\mathcal{N}(a,b)$ and $\mathcal{CN}(a,b)$ indicate real-valued and complex-valued Gaussian processes with mean a and variance b. The PDF and the cumulative distribution function (CDF) of the standard normal distribution are denoted by $\phi(x) \triangleq \frac{1}{\sqrt{2\pi}}\exp\left[-x^2/2\right]$ and

$\Phi(x) \triangleq \int_{-\infty}^{x} \phi(v)dv$, respectively.

II. System model

A. Signal model

Consider an uplink large MU-MIMO system composed of a BS having N' receive (RX) antennas and serving M' ($\leq N'$) synchronized user equipment (UE) devices with single-antenna. We employ quadrature amplitude modulation (QAM), with the m'-th UE conveying a modulated symbol $x'_{m'}$ that represents one of Q' constellation points $\mathcal{X}' \triangleq \left\{\chi'_1, \ldots, \chi'_{q'}, \ldots, \chi'_{Q'}\right\}$, where the average power density is denoted by E_s. Accordingly, the RX vector is given by

$$\boldsymbol{y}' \triangleq \boldsymbol{H}'\boldsymbol{x}' + \boldsymbol{z}', \tag{1}$$

where $\boldsymbol{x}' \in \mathcal{X}^{\mathrm{c}\ M'\times 1}$ denotes a transmit (TX) vector, $\boldsymbol{H}' \in \mathbb{C}^{N'\times M'}$ denotes a $N' \times M'$ MIMO channel matrix, and $\boldsymbol{z}' \in \mathbb{C}^{N'\times 1}$ is a circularly symmetric zero-mean i.i.d. additive white Gaussian noise (AWGN), where $\mathbb{E}_{\boldsymbol{z}'}\left\{\boldsymbol{z}'\boldsymbol{z}'^{\mathrm{H}}\right\} = N_0\boldsymbol{I}_{N'}$.

Without loss of generality, $\boldsymbol{H}'$ in (1) can be represented by a geometric channel model with L scatters in mmWave channels [20], where each scatter contributes to a single propagation path between the BS and the UEs. Accordingly, the m'-th column vector of $\boldsymbol{H}'$ can be expressed as

$$\boldsymbol{h}'_{m'} = \frac{1}{\sqrt{L}}\sum_{l=1}^{L} \alpha_{m',l}\boldsymbol{a}_{m',l}(\omega_{m',l}), \tag{2}$$

where $\alpha_{m',l}$ is the channel gain along the l-th path of the m'-th UE. This is obtained from the antenna steering vector $\boldsymbol{a}(\omega_{m',l}) \triangleq \left[1, e^{\mathrm{j}\omega_{m',l}}, \ldots, e^{\mathrm{j}(N'-1)\omega_{m',l}}\right]^{\mathrm{T}}$, where $\omega_{m',l} \triangleq \pi \sin\zeta_{m',l}$ with $\zeta_{m',l}$ denoting the azimuth angle of arrival (AoA) of the l-th path of the m'-th UE. The antenna element space is fixed to half the wavelength.

For ease of algebraic manipulations, the complex-valued signal model of (1) can be transformed into a double-sized real-valued signal model on the basis of pulse amplitude modulation (PAM) symbols [21] as follows

$$\boldsymbol{y} = \boldsymbol{H}\boldsymbol{x} + \boldsymbol{z}, \tag{3}$$

where

$$\boldsymbol{y} \triangleq \begin{bmatrix}\Re\{\boldsymbol{y}'\}\\ \Im\{\boldsymbol{y}'\}\end{bmatrix} \in \mathbb{C}^{N\times 1},\ \boldsymbol{H} \triangleq \begin{bmatrix}\Re\{\boldsymbol{H}'\} & -\Im\{\boldsymbol{H}'\}\\ \Im\{\boldsymbol{H}'\} & \Re\{\boldsymbol{H}'\}\end{bmatrix} \in \mathbb{C}^{N\times M},$$
$$\boldsymbol{x} \triangleq \begin{bmatrix}\Re\{\boldsymbol{x}'\}\\ \Im\{\boldsymbol{x}'\}\end{bmatrix} \in \mathcal{X}^{M\times 1},\ \boldsymbol{z} \triangleq \begin{bmatrix}\Re\{\boldsymbol{z}'\}\\ \Im\{\boldsymbol{z}'\}\end{bmatrix} \in \mathbb{C}^{N\times 1}, \tag{4}$$

with $M \triangleq 2M'$ and $N \triangleq 2N'$. The m-th PAM symbol x_m in $\boldsymbol{x}$ represents one of Q ($\triangleq \sqrt{Q'}$) PAM constellation points $\mathcal{X} \triangleq \left\{\chi_1, \ldots, \chi_q, \ldots, \chi_Q\right\}$ whose entries are amplitudes of the real and imaginary components of $\mathcal{X}'$. Let us define a coefficient $c \triangleq \sqrt{3E_s/(2(Q'-1))}$ for normalizing the average power density of χ_q to $E_s/2$. For example, in the 4QAM case ($Q' = 4$, $Q = 2$), we have $\mathcal{X} = \{\pm c\}$ and $c = \sqrt{E_s/2}$.

B. Quantization with low-resolution ADCs

The in-phase and quadrature components of the signal received by each antenna are individually quantized by an ADC with b-bit resolution. The ADC can be characterized by a set of 2^b+1 quantization thresholds $\mathcal{T}_b \triangleq \{\tau_0, \tau_1, \ldots, \tau_{2^b}\}$, such that $-\infty = \tau_0 < \tau_1 < \cdots < \tau_{2^b} = \infty$, and a set of 2^b representative values $\mathcal{L}_b \triangleq \{l_0, l_1, \ldots, l_{2^b-1}\}$ where $l_i \in (\tau_i, \tau_{i+1}]$. The operation of the N b-bit ADCs at the BS can be represented by the quantization function $Q_b^N(\cdot) : \mathbb{R}^N \to \mathcal{L}_b^N$ that maps the RX vector $\boldsymbol{y}$ to the quantized output $\boldsymbol{r}$ as

$$\boldsymbol{r} \triangleq [r_1, \ldots, r_N]^{\mathrm{T}} = Q_b^N(\boldsymbol{y}) = Q_b^N(\boldsymbol{H}\boldsymbol{x} + \boldsymbol{z}), \tag{5}$$

where the n-th output is given by

$$r_n = Q_b^1(y_n) = l_i \text{ if } y_n \in (\tau_i, \tau_{i+1}]. \tag{6}$$

C. Linearization based on Bussgang theorem

Using finite-resolution ADCs induces a signal distortion that is correlated with the input to the quantizer, which is intractable for subsequent stochastic signal processing. To circumvent this issue, when the quantizer input follows a Gaussian distribution, we can exploit the Bussgang theorem [11] to transform the quantized output $\boldsymbol{r}$ of (5) into

$$\boldsymbol{r} = \boldsymbol{G}\boldsymbol{y} + \boldsymbol{d}, \tag{7}$$

where $\boldsymbol{G}$ and $\boldsymbol{d}$ are the linear operator and the equivalent quantizer noise, respectively. $\boldsymbol{G}$ is chosen to make $\boldsymbol{d}$ uncorrelated with $\boldsymbol{y}$. Regarding the $\boldsymbol{y} \sim \mathcal{CN}(\boldsymbol{0}_{N\times 1}, \tilde{\boldsymbol{C}}_{\mathrm{yy}})$, *i.e.*, $\tilde{\boldsymbol{C}}_{\mathrm{yy}} \triangleq \mathbb{E}_{\boldsymbol{y}}\left\{\boldsymbol{y}\boldsymbol{y}^{\mathrm{T}}\right\}$, it follows from (7) that [4]

$$\boldsymbol{G} = \sum_{i=0}^{2^b-1} \frac{l_i}{\sqrt{2\pi\psi^{\mathrm{y}}}}\left(\mathrm{e}^{-\frac{\tau_i^2}{2\psi^{\mathrm{y}}}} - \mathrm{e}^{\frac{\tau_{i+1}^2}{2\psi^{\mathrm{y}}}}\right)\boldsymbol{I}_N \triangleq g\boldsymbol{I}_N, \tag{8}$$

where $\mathrm{diag}\left(\tilde{\boldsymbol{C}}_{\mathrm{yy}}\right) = \psi^{\mathrm{y}}\boldsymbol{I}_N$.

D. Linear MMSE based on Bussgang theorem

From (5), the BMMSE detector is given by solving the following optimization problem: [3], [5]

$$\boldsymbol{W} = \arg\min_{\underline{\boldsymbol{W}}} \underbrace{\mathbb{E}_{\mathbf{x},\mathbf{z}}\left\{\|\underline{\boldsymbol{W}}^{\mathrm{T}}\boldsymbol{r} - \boldsymbol{x}\|^2\right\}}_{J(\underline{\boldsymbol{W}})}. \tag{9}$$

The resulting detector can be found from the solution of derivative: $\frac{\partial J(\boldsymbol{W})}{\partial \boldsymbol{W}^{\mathrm{T}}} = 0$ as

$$\boldsymbol{W} = \boldsymbol{C}_{\mathrm{rr}}^{-1}\mathbb{E}_{\mathbf{x},\mathbf{z}}\left\{\boldsymbol{r}\boldsymbol{x}^{\mathrm{T}}\right\} = \frac{gE_s}{2}\boldsymbol{C}_{\mathrm{rr}}^{-1}\boldsymbol{H}, \tag{10}$$

where $\boldsymbol{C}_{\mathrm{rr}} \triangleq \mathbb{E}_{\mathbf{x},\mathbf{z}}\left\{\boldsymbol{r}\boldsymbol{r}^{\mathrm{T}}\right\}$ can be computed in two ways. One is based on the arcsine law, which is available only for the 1-bit quantization case. It has been shown in [22] that

$$\boldsymbol{C}_{\mathrm{rr}} = \frac{2\psi^{\mathrm{y}}}{\pi}\left(\arcsin\left[\mathrm{diag}\left(\boldsymbol{C}_{\mathrm{yy}}\right)^{-\frac{1}{2}}\boldsymbol{C}_{\mathrm{yy}}\mathrm{diag}\left(\boldsymbol{C}_{\mathrm{yy}}\right)^{-\frac{1}{2}}\right]\right), \tag{11}$$

where $\boldsymbol{C}_{\mathrm{yy}} \triangleq \mathbb{E}_{\mathbf{x},\mathbf{z}}\left\{\boldsymbol{y}\boldsymbol{y}^{\mathrm{T}}\right\} = \frac{1}{2}\left[E_s\boldsymbol{H}\boldsymbol{H}^{\mathrm{T}} + N_0\boldsymbol{I}_N\right]$. The other is based on the averaging and diagonal approximation of $\boldsymbol{C}_{\mathrm{dd}} \triangleq \mathbb{E}_{\mathbf{x},\mathbf{z}}\left\{\boldsymbol{d}\boldsymbol{d}^{\mathrm{T}}\right\} \approx \mathrm{diag}\left(\mathbb{E}_{\boldsymbol{y}}\left\{\boldsymbol{d}\boldsymbol{d}^{\mathrm{T}}\right\}\right)$ [4]; thus, we simply ignore the temporal correlation of the quantizer, leading to [8]

$$\boldsymbol{C}_{\mathrm{rr}} \approx g^2 \cdot \boldsymbol{C}_{\mathrm{yy}} + \left(1 - g^2\right)\psi^{\mathrm{y}}\boldsymbol{I}_N, \tag{12}$$

which can be used for multi-bit quantization.

III. MPDQ via GaBP based on Bussgang's Theorem

In this section, we describe the algorithmic structure of MPDQ via GaBP based on the Bussgang theorem. It consists of two estimation procedures, namely, the de-quantization (DQ) step and the MUD step. The DQ step recovers the RX vector $\boldsymbol{y}$ based on $\boldsymbol{r}$ and *soft replicas* (*i.e.*, tentative estimates) of the TX vector generated in the previous iteration, and then estimates $\boldsymbol{d}$. The MUD step estimates the TX vector $\boldsymbol{x}$ based on $\boldsymbol{r}$ and soft replicas of $\boldsymbol{x}$ and $\boldsymbol{d}$ via three modules: soft interference canceler (soft IC), belief generator (BG), and soft

replica generator (soft RG). The soft IC performs for each RX symbol by subtracting inter-user interference (IUI) and quantization distortion with the soft replicas generated in the previous iteration. The BG approximates the effective noise in *beliefs* (*i.e.*, information propagated across iterations) as i.i.d. Gaussian noise based on the central limit theorem (CLT); this behavior is referred to as scalar Gaussian approximation (SGA). Finally, under the SGA condition, the soft RG approximately calculates the soft replica based on the conditional expectation of the TX symbol.

The soft replicas of x_m and y_n are respectively defined as $\{\check{x}_{n,m}, \forall n\}$ and $\{\check{y}_{n,m}, \forall m\}$, and their mean square errors (MSEs) are respectively denoted by

$$\check{\psi}^{\mathrm{x}}_{n,m} \triangleq \mathbb{E}_{\tilde{\mathrm{x}}_{n,m}}\left\{\tilde{x}^2_{n,m}\right\}, \quad \because x_m = \check{x}_{n,m} + \tilde{x}_{n,m}, \tag{13}$$

$$\check{\psi}^{\mathrm{y}}_{n,m} \triangleq \mathbb{E}_{\tilde{\mathrm{y}}_{n,m}}\left\{\tilde{y}^2_{n,m}\right\}, \quad \because y_n = \check{y}_{n,m} + \tilde{y}_{n,m}. \tag{14}$$

where $\{\tilde{x}_{n,m}, \forall n\}$ and $\{\tilde{y}_{n,m}, \forall m\}$ are estimation errors. From (7) and (14), the distortion can be expressed as

$$d_n = r_n - g y_n = \underbrace{r_n - g\check{y}_{n,m}}_{\check{d}_{n,m}} \underbrace{-g\tilde{y}_{n,m}}_{\tilde{d}_{n,m}} = \check{d}_{n,m} + \tilde{d}_{n,m}, \tag{15}$$

where the MSE of $\check{d}_{n,m}$ is given by

$$\psi^{\mathrm{d}}_{n,m} \triangleq \mathbb{E}_{\tilde{\mathrm{y}}_{n,m}}\left\{\tilde{d}^2_{n,m}\right\} = g^2\check{\psi}^{\mathrm{y}}_{n,m}. \tag{16}$$

A. DQ step

At the first iteration ($k = 1$), *i.e.*, the soft replica is not available as prior information, the soft replica $\{\check{y}_{n,m}, \forall m\}$ are given by the conditional expectation as

$$\check{y}_{n,m} = \int y_n p_{\mathrm{y}_n|\mathrm{r}_n}(y_n|r_n)\, dy_n, \ \forall m. \tag{17}$$

Owing to the CLT in the large-system condition, the PDF of y_n can be expressed as

$$p_{\mathrm{y}_n}(y_n) = \frac{1}{\sqrt{2\pi\psi^{\mathrm{y}}_n}} \exp\left[-\frac{y_n^2}{2\psi^{\mathrm{y}}_n}\right]. \tag{18}$$

In this case, the conditional PDF in (17) can be expressed with the truncated Gaussian distribution as

$$p_{\mathrm{y}_n|\mathrm{r}_n}(y_n|r_n = l_i) = \frac{p_{\mathrm{y}_n}(y_n)}{\int_{\tau_i}^{\tau_{i+1}} p_{\mathrm{y}_n}(y_n)\, dy_n}, \tag{19}$$

where $y_n \in (\tau_i, \tau_{i+1}]$. From the mean and variance of (19), the estimate and MSE are respectively given by

$$\check{y}_{n,m} = \eta\left(y_n; 0, \sqrt{\psi^{\mathrm{y}}_n}, \tau_i, \tau_{i+1}\right), \ \forall m, \tag{20a}$$

$$\check{\psi}^{\mathrm{y}}_{n,m} = \zeta\left(y_n; 0, \sqrt{\psi^{\mathrm{y}}_n}, \tau_i, \tau_{i+1}\right), \ \forall m, \tag{20b}$$

where $\eta(\cdot)$ and $\zeta(\cdot)$ are functions that calculate the mean and variance of a truncated Gaussian distribution, respectively, as

$$\eta(u; \mu, \sigma, a, b) = \mu + \sigma\frac{\phi(\alpha) - \phi(\beta)}{\Phi(\beta) - \Phi(\alpha)}, \tag{21a}$$

$$\zeta(u; \mu, \sigma, a, b) = \sigma^2\left[1 + \frac{\alpha\phi(\alpha) - \beta\phi(\beta)}{\Phi(\beta) - \Phi(\alpha)} - \left(\frac{\phi(\alpha) - \phi(\beta)}{\Phi(\beta) - \Phi(\alpha)}\right)^2\right], \tag{21b}$$

with $\alpha = \frac{a-\mu}{\sigma}$ and $\beta = \frac{b-\mu}{\sigma}$.

At the second and later iterations ($k \neq 1$), the soft replica is available as prior information; therefore, instead of (17), we should consider the following conditional expectation:

$$\check{y}_{n,m} = \int y_n p_{\mathrm{y}_n|\check{\tilde{\mathbf{x}}}_{n,m},\mathrm{r}_n}\left(y_n|\check{\tilde{\boldsymbol{x}}}_{n,m}, r_n\right) dy_n, \tag{22}$$

where $\check{\tilde{\boldsymbol{x}}}_{n,m} = \left[\check{x}_{n,1}, \ldots, \check{x}_{n,m-1}, 0, \check{x}_{n,m+1}, \ldots, \check{x}_{n,M}\right]^{\mathrm{T}}$. Assuming that $\check{\tilde{\boldsymbol{x}}}_{n,m}$ and r_n are independent of each other, the conditional PDF in (22) can be rewritten as

$$p_{\mathrm{y}_n|\check{\tilde{\mathbf{x}}}_{n,m},\mathrm{r}_n}\left(y_n|\check{\tilde{\boldsymbol{x}}}_{n,m}, r_n\right) = \frac{1}{p_{\mathrm{y}_n}(y_n)} p_{\mathrm{y}_n|\check{\tilde{\mathbf{x}}}_{n,m}}\left(y_n|\check{\tilde{\boldsymbol{x}}}_{n,m}\right) p_{\mathrm{y}_n|\mathrm{r}_n}(y_n|r_n). \tag{23}$$

Substituting (19) into (23),

$$p_{\mathrm{y}_n|\check{\tilde{\mathbf{x}}}_{n,m},\mathrm{r}_n}\left(y_n|\check{\tilde{\boldsymbol{x}}}_{n,m}, r_n = l_i\right) = C^{(i)}_{n,m} \cdot \frac{p_{\mathrm{y}_n|\check{\tilde{\mathbf{x}}}_{n,m}}\left(y_n|\check{\tilde{\boldsymbol{x}}}_{n,m}\right)}{\int_{\tau_i}^{\tau_{i+1}} p_{\mathrm{y}_n|\check{\tilde{\mathbf{x}}}_{n,m}}\left(y_n|\check{\tilde{\boldsymbol{x}}}_{n,m}\right) dy_n}, \tag{24}$$

with $C^{(i)}_{n,m} = \frac{\int_{\tau_i}^{\tau_{i+1}} p_{y_n|\check{\tilde{\mathbf{x}}}_{n,m}}\left(y_n|\check{\tilde{\boldsymbol{x}}}_{n,m}\right) dy_n}{\int_{\tau_i}^{\tau_{i+1}} p_{\mathrm{y}_n}(y_n) dy_n}$ is a proportionality constant; thus, (24) is the truncated Gaussian distribution. To find the truncated distribution in (24), with the use of the soft replicas, the RX symbol can be rewritten as

$$\begin{aligned} y_n &= \underbrace{\sum_{i\neq m} h_{n,i}\check{x}_{n,i} + h_{n,m}x_m + \sum_{i\neq m} h_{n,i}\tilde{x}_{n,i} + z_n}_{\triangleq \nu^{\mathrm{s}}_{n,m}\text{: SGA of the effective noise}} \\ &\approx \sum_{i\neq m} h_{n,i}\check{x}_{n,i} + \nu^{\mathrm{s}}_{n,m} \triangleq \tilde{s}_{n,m}. \end{aligned} \tag{25}$$

Accordingly, the conditional PDF given $\check{\tilde{\boldsymbol{x}}}_{n,m}$ is given by

$$p_{\mathrm{y}_n|\check{\tilde{\mathbf{x}}}_{n,m}}\left(y_n|\check{\tilde{\boldsymbol{x}}}_{n,m}\right) \propto \exp\left[-\frac{\left(\tilde{s}_{n,m} - \sum_{i\neq m} h_{n,i}\check{x}_{n,i}\right)^2}{2\psi^{\mathrm{s}}_{n,m}}\right], \tag{26}$$

with the variance of $\nu^{\mathrm{s}}_{n,m}$:

$$\psi^{\mathrm{s}}_{n,m} = \sum_{i\neq m} h^2_{n,i}\check{\psi}^{\mathrm{x}}_{n,i} + \frac{1}{2}\left(E_{\mathrm{s}}h^2_{n,m} + N_0\right). \tag{27}$$

From (22), (24), (25), and (27), we have

$$\check{y}_{n,m} = \eta\left(y_n; \sum_{i\neq m} h_{n,i}\check{x}_{n,i}, \sqrt{\psi^{\mathrm{s}}_{n,m}}, \tau_i, \tau_{i+1}\right), \tag{28a}$$

$$\check{\psi}^{\mathrm{y}}_{n,m} = \zeta\left(y_n; \sum_{i\neq m} h_{n,i}\check{x}_{n,i}, \sqrt{\psi^{\mathrm{s}}_{n,m}}, \tau_i, \tau_{i+1}\right). \tag{28b}$$

B. MUD step

1) Soft IC: Focusing on the soft IC for the n-th RX symbol y_n, with the soft replicas $\{\check{x}_{n,m}, \check{d}_{n,m}, \forall m, n\}$ generated in the previous iteration. Note that $\check{x}_{n,m} = 0, \forall m, n$ at the first iteration. In the detection of an arbitrary TX symbol x_m, the cancellation process is performed with the aid of (7) as

$$\begin{aligned} \tilde{r}_{n,m} &= r_n - g\sum_{i\neq m} h_{n,i}\check{x}_{n,i} - \check{d}_{n,m} \\ &= gh_{n,m}x_m + \underbrace{g\sum_{i\neq m} h_{n,i}\tilde{x}_{n,i} + gz_n + \tilde{d}_{n,m}}_{\triangleq \nu^{\mathrm{r}}_{n,m}\text{: SGA of the effective noise}}. \end{aligned} \tag{29}$$

Accordingly, the conditional PDF of $\tilde{r}_{n,m}$ is given by

$$p_{\tilde{\mathsf{r}}_{n,m}|\mathsf{x}_m}\left(\tilde{r}_{n,m}|x_m\right) \propto \exp\left[-\frac{\left(\tilde{r}_{n,m}-gh_{n,m}x_m\right)^2}{2\psi^{\mathrm{r}}_{n,m}}\right], \tag{30}$$

where from (14) and (15) we have the variance of $\nu^{\mathrm{r}}_{n,m}$ as

$$\psi^{\mathrm{r}}_{n,m} = g^2\left(\sum_{i\neq m} h^2_{n,i}\check{\psi}^{\mathrm{x}}_{n,m} + \frac{N_0}{2}\right) + \psi^{\mathrm{d}}_{n,m}. \tag{31}$$

2) BG: Assuming that the effective noise in $\left\{\tilde{r}_{n,m}, \forall m, n\right\}$ are not correlated to each other owing to the high-precision SGA, the extrinsic belief $l_{n.m}$ for x_m is simply obtained by

$$p_{\mathsf{l}_{n,m}|\mathsf{x}_m}\left(l_{n,m}|x_m\right) = \prod_{i\neq n} p_{\tilde{\mathsf{r}}_{i,m}|\mathsf{x}_m}\left(\tilde{r}_{i,m}|x_m\right)$$

$$\propto \exp\left[-\sum_{i\neq n}\frac{\left(\tilde{r}_{i,m}-gh_{i,m}x_m\right)^2}{2\psi^{\mathrm{r}}_{i,m}}\right]. \tag{32}$$

3) Soft RG: Similarly, assuming that the effective noise in $\left\{l_{n,m}, \forall m, n\right\}$ are not correlated to each other under the SGA, from Bayes' rule, the soft replica can be in general obtained from the symbol-wise conditional expectation as [18]

$$\check{x}_{n,m} = \sum_{\chi_q}\chi_q\frac{p_{\mathsf{l}_{n,m}|\mathsf{x}_m}\left(l_{n,m}|\chi_q\right)}{\sum_{\underline{\chi}_q} p_{\mathsf{l}_{n,m}|\underline{\chi}_q}\left(l_{n,m}|\underline{\chi}_q\right)}, \tag{33a}$$

$$\psi^{\mathrm{x}}_{n,m} = \sum_{\chi_q}\chi_q^2\frac{p_{\mathsf{l}_{n,m}|\mathsf{X}_m}\left(l_{n,m}|\chi_q\right)}{\sum_{\underline{\chi}_q} p_{\mathsf{l}_{n,m}|\underline{\chi}_q}\left(l_{n,m}|\underline{\chi}_q\right)} - \check{x}^2_{n,m}. \tag{33b}$$

When the number of iterations reaches the predetermined value K, x_m is hard-detected as

$$\hat{x}_m = \arg\min_{\chi_q}\left\{\sum_{n=1}^{N}\frac{\left(\tilde{r}_{n,m}-gh_{n,m}\chi_q\right)^2}{2\psi^{\mathrm{r}}_{n,m}}\right\}. \tag{34}$$

C. Belief scaling

Although the large-system approximation is relaxed compared to the GAMP-based MPDQ, the operation principle of the proposed method still relies on the high-precision SGA brought by large-system conditions. Therefore, an adaptively scaled belief (ASB), which was proposed in [18] to stabilize the GaBP iterative behavior, is introduced.

The extrinsic likelihood function in (32) can be rewritten as

$$p_{\mathsf{l}_{n,m}|\mathsf{x}_m}\left(l_{n,m}|\chi_q\right) \propto \exp\left[\lambda_{n,m}(\chi_q)\right], \tag{35}$$

where we define

$$\lambda_{n,m}(\chi_q) \triangleq \chi_q\left(o_{n,m}-\frac{1}{2}\omega_{n,m}\chi_q\right). \tag{36}$$

with

$$o_{n,m} = \sum_{i\neq n}^{N}\frac{gh_{i,m}\tilde{r}_{i,m}}{\psi^{\mathrm{r}}_{i,m}}, \quad \omega_{n,m} = \sum_{i\neq n}^{N}\frac{g^2h^2_{i,m}}{\psi^{\mathrm{r}}_{i,m}}. \tag{37}$$

The ASB is given by scaling the belief $\lambda_{n,m}$ after normalizing the belief with its effective gain as

$$\lambda'_{n,m}\left(\chi_q\right) = \frac{\epsilon}{c^2\omega_{n,m}}\lambda_{n,m}\left(\chi_q\right)$$

$$= \chi_q\left(\gamma_{n,m}-\frac{1}{2}\chi_q\right)\frac{\epsilon}{c^2}, \quad \because \gamma_{n,m} = \frac{o_{n,m}}{\omega_{n,m}}, \tag{38}$$

where ϵ is a scaling parameter whose dynamics is given by the following simple function as $\epsilon(k) = \kappa_1\cdot\left(\frac{k}{K}\right)^{\kappa_2}$ [18], where

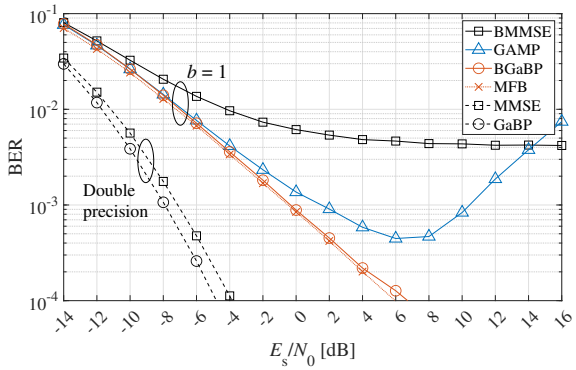

(a) $b = 1$ case

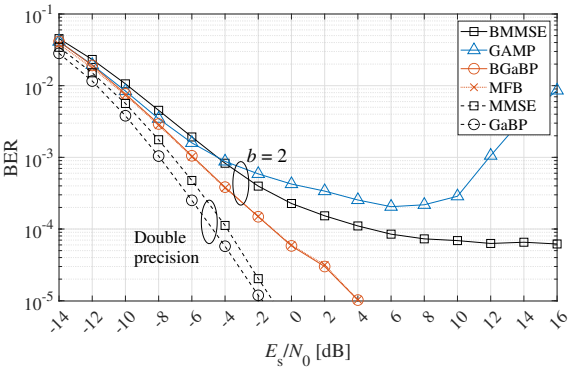

(b) $b = 2$ case

Fig. 1. BER performances of every detector for $b = 1$ and 2 in the MU-MIMO system with $(N', M') = (128, 16)$ configuration.

κ_1 and κ_2 are the predetermined parameters. The resulting soft RG is given by

$$\check{x}_{n,m} = \sum_{\chi_q}\chi_q\frac{\exp\left[\frac{\epsilon}{c^2}\cdot\chi_q\left(\gamma_{n,m}-\frac{1}{2}\chi_q\right)\right]}{\sum_{\underline{\chi}_q}\exp\left[\frac{\epsilon}{c^2}\cdot\underline{\chi}_q\left(\gamma_{n,m}-\frac{1}{2}\underline{\chi}_q\right)\right]}. \tag{39}$$

The proposed algorithm consists of only scalar-by-scalar operation, which is of order $O(NM)$ per iteration, which is the same as those of the GAMP-based MPDQ [14]–[16].

IV. Numerical Results

In this section, computer simulations are conducted for evaluations of the proposed GaBP-based MPDQ algorithm in large mmWave MU-MIMO systems with low-resolution ADCs, comparing it to the SotA alternatives, *i.e.*, the BMMSE [3]–[5] detector and the GAMP-based MPDQ detector [14].

In (2), the number of paths is set to $L = 4$ and each gain is set to $\alpha_{m',l} \sim \mathcal{CN}(0, 1)$ on the basis of slow TX power control. In order to focus on the MUD performance, $\boldsymbol{H}'$ is assumed to be perfectly known on the BS side. The modulation scheme is Gray-coded quadrature phase-shift keying (QPSK), and channel coding is not utilized. The MSE-optimal quantizer using the Lloyd-Max algorithm is used. The number of MPDQ iterations is set to $K = 16$. Several simulations were conducted to find sub-optimal (κ_1, κ_2) for minimizing the required E_s/N_0 at BER $= 10^{-5}$, and then we set $(\kappa_1, \kappa_2) = (10, 2)$.

A. BER performance

Fig. 1 shows BER performance of every detector for $b = 1$ and 2 in the MU-MIMO system with $(N', M') = (128, 16)$ configuration. As a reference, the performances of typical

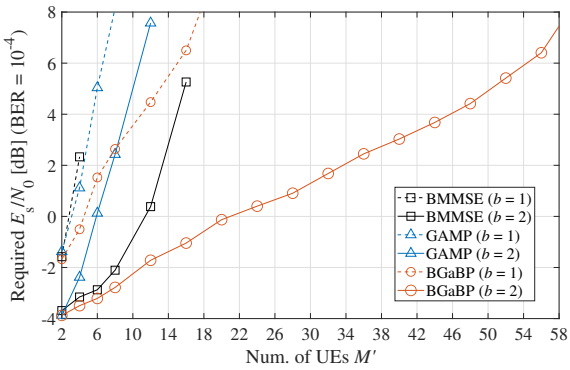

Fig. 2. Required E_s/N_0 for achieving a BER of less than 10^{-4} according to at M' for $N' = 128$.

linear MMSE detector and GaBP detector [18] with the double-precision ADCs (*i.e.*, unquantization), "MMSE" and "GaBP", are respectively presented. In addition, "MFB" shows an idealized (genie-aided) performance which is achieved only when the knowledge of $\boldsymbol{x}$ is perfectly known as the prior information in the proposed method [23].

The BMMSE detector, "BMMSE", and the GAMP-based MPDQ method [14], "GAMP", suffer from high-level error floors in the $b = 1$ case in Fig. 1(a) due to severe quantization distortion, although reducing the number of quantization bits is the very aim of the methods themselves. Even in the $b = 2$ case in Fig. 1(b), "GAMP" still suffers an error floor due to spatial fading correlation, and even "BMMSE" cannot completely suppress an error floor because of the lack of a DQ mechanism. In contrast, the proposed MPDQ method, "Bussgang GaBP (BGaBP)", achieves BER = 10^{-4} without an error floor even in the $b = 1$ case in Fig. 1(a), approaching the performance of "MFB." Furthermore, Fig. 1(b) shows that the degradation from "GaBP" is reduced to only about 2 dB at BER = 10^{-4}. These results suggest that our proposed method can maintain reliable signal detection with quite few quantization bits ($b \leq 2$) even in the correlated mmWave MU-MIMO systems, owing to the robust signal recovery capability resulting from the GaBP approach with belief scaling.

Let us shift our focus to other MU-MIMO configurations. Fig. 2 shows the E_s/N_0 required to guarantee a BER of less than 10^{-4} as a function of the number of UEs M', while fixing the number of RX antennas at $N' = 128$. The other settings are the same as in Fig. 1. Obviously, "GAMP" cannot support a high number of UEs due to errors in *Onsager correction* under correlated mmWave channel conditions. Owing to the high-level error floor, it can achieve a BER of 10^{-4} only when $M \leq 8$ for $b = 1$ and $M \leq 12$ for $b = 2$. In contrast, "BMMSE" can support a larger number of UEs thanks to the whitening mechanism as b increases. However, the required E_s/N_0 increases more rapidly than in "BGaBP." The gain of the proposed method for "BMMSE" increases with higher spatial-loading configurations; this is due to the iterative gain of MPDQ, which is robust against spatial fading correlation.

V. Conclusion

In this paper, we propose a novel MPDQ algorithm via GaBP based on the Bussgang theorem for uplink signal detection in mmWave large MU-MIMO systems with low-resolution ADCs. The proposed scheme consists of the DQ step estimating the quantization distortions based on the truncated Gaussian distribution and the MUD step estimating the data symbols based on the GaBP approach, and the extrinsic beliefs and soft replicas are exchanged between them to achieve robust signal recovery. The advantages of the proposed scheme over SotA alternatives in terms of BER performance are confirmed via software simulation.

Acknowledgement

A part of this work was supported by JSPS KAKENHI Grant Number JP20K14734 and JP21H01332, Japan.

References

[1] M. Xiao *et al.*, "Millimeter wave communications for future mobile networks," *IEEE J-SAC*, vol. 35, no. 9, pp. 1909–1935, 2017.
[2] C. Studer and G. Durisi, "Quantized massive MU-MIMO-OFDM uplink," *IEEE Trans. Commun.*, vol. 64, no. 6, pp. 2387–2399, 2016.
[3] Y. Li *et al.*, "Channel estimation and performance analysis of one-bit massive MIMO systems," *IEEE Trans. Signal Processing*, vol. 65, no. 15, pp. 4075–4089, 2017.
[4] S. Jacobsson, G. Durisi, M. Coldrey, *et al.*, "Throughput analysis of massive MIMO uplink with low-resolution ADCs," *IEEE Trans. Wireless Commun.*, vol. 16, no. 6, pp. 4038–4051, 2017.
[5] L. V. Nguyen, A. L. Swindlehurst, and D. H. N. Nguyen, "Linear and deep neural network-based receivers for massive MIMO systems with one-bit ADCs," *IEEE Trans. Wireless Commun.*, vol. 20, no. 11, pp. 7333–7345, 2021.
[6] J. Mo, P. Schniter, and R. W. Heath, "Channel estimation in broadband millimeter wave MIMO systems with few-bit ADCs," *IEEE Trans. Signal Processing*, vol. 66, no. 5, pp. 1141–1154, 2018.
[7] S. Rao, A. Mezghani, and A. L. Swindlehurst, "Channel estimation in one-bit massive MIMO systems: Angular versus unstructured models," *IEEE J-STSP*, vol. 13, no. 5, pp. 1017–1031, 2019.
[8] I. Atzeni and A. Tölli, "Channel estimation and data detection analysis of massive MIMO with 1-bit ADCs," *IEEE Trans. Wireless Commun.*, pp. 1–1, 2021.
[9] Choi *et al.*, "Near maximum-likelihood detector and channel estimator for uplink multiuser massive MIMO systems with one-bit ADCs," *IEEE Trans. Commun.*, vol. 64, no. 5, pp. 2005–2018, 2016.
[10] Y.-S. Jeon, N. Lee, S.-N. Hong, and R. W. Heath, "One-bit sphere decoding for uplink massive MIMO systems with one-bit ADCs," *IEEE Trans. Wireless Commun.*, vol. 17, no. 7, pp. 4509–4521, 2018.
[11] J. J. Bussgang, "Crosscorrelation functions of amplitude-distorted gaussian signals," *Tech. Rep. 216, Research Lab. Electron*, 1952.
[12] Z. Shao, R. C. de Lamare, and L. T. N. Landau, "Iterative detection and decoding for large-scale multiple-antenna systems with 1-bit ADCs," *IEEE Wireless Commun. Letters*, vol. 7, no. 3, pp. 476–479, 2018.
[13] Mezghani *et al.*, "Belief propagation based MIMO detection operating on quantized channel output," in *IEEE ISIT*, 2010, pp. 2113–2117.
[14] U. S. Kamilov, V. K. Goyal, and S. Rangan, "Message-passing dequantization with applications to compressed sensing," *IEEE Trans. Signal Processing*, vol. 60, no. 12, pp. 6270–6281, 2012.
[15] T.-C. Zhang, C.-K. Wen, S. Jin, and T. Jiang, "Mixed-ADC massive MIMO detectors: Performance analysis and design optimization," *IEEE Tran. Wireless Commun.*, vol. 15, no. 11, pp. 7738–7752, 2016.
[16] Z. Zhang, X. Cai, C. Li, C. Zhong, and H. Dai, "One-bit quantized massive MIMO detection based on variational approximate message passing," *IEEE Trans. Sig. Process.*, vol. 66, no. 9, pp. 2358–2373, 2018.
[17] X. Meng, S. Wu, and J. Zhu, "A unified bayesian inference framework for generalized linear models," *IEEE Signal Processing Letters*, vol. 25, no. 3, pp. 398–402, 2018.
[18] T. Takahashi, S. Ibi, and S. Sampei, "Design of adaptively scaled belief in multi-dimensional signal detection for higher-order modulation," *IEEE Trans, Commun.*, vol. 67, no. 3, pp. 1986–2001, Mar. 2019.
[19] H. Iimori *et al.*, "Grant-free access via bilinear inference for cell-free MIMO with low-coherence pilots," *IEEE Trans. Wireless Commun.*, vol. 20, no. 11, pp. 7694–7710, 2021.
[20] D. Fan *et al.*, "Angle domain channel estimation in hybrid millimeter wave massive MIMO systems," *IEEE Trans. Wireless Commun.*, vol. 17, no. 12, pp. 8165–8179, 2018.
[21] A. Chockalingam and B. S. Rajan, *Large MIMO Systems*. Cambridge University Press, 2014.
[22] A. Mezghani and J. A. Nossek, "Capacity lower bound of MIMO channels with output quantization and correlated noise," in *IEEE ISIT*, 2012, pp. 1–6.
[23] T. Takahashi, A. Tölli, S. Ibi, and S. Sampei, "Low-complexity large MIMO detection via layered belief propagation in beam domain," *IEEE Trans, Wireless Commun.*, vol. 21, no. 1, pp. 234–249, 2022.